The Cryosphere Discuss., 7, 5683–5709, 2013
www.the-cryosphere-discuss.net/7/5683/2013/
doi:10.5194/tcd-7-5683-2013

The Cryosphere Discussions
Open Access

Modeling the response of Lambert Glacier–Amery Ice Shelf system, East Antarctic, to uncertain climate forcing over the 21st and 22nd centuries

Y. Gong[1,2], S. L. Cornford[3], and A. J. Payne[3]

[1]School of Earth Sciences, University of Bristol, Bristol, UK
[2]Arctic Centre, Lapland University, Rovaniemi, Finland
[3]School of Geographical Sciences, University of Bristol, Bristol, UK

Received: 23 October 2013 – Accepted: 31 October 2013 – Published: 2 December 2013

Correspondence to: A. J. Payne (a.j.payne@bristol.ac.uk)

Published by Copernicus Publications on behalf of the European Geosciences Union.

Abstract

The interaction between the climate system and the large polar ice sheets regions is a key process in global environmental change. We carried out ice dynamic simulations of one of the largest drainage systems in East Antarctica: the Lambert Glacier–Amery Ice Shelf system, with an adaptive mesh ice sheet model. The ice sheet model is driven by surface accumulation and basal melt rates computed by two ocean and two atmosphere models. The change of the ice thickness and velocity in the ice shelf is mainly influenced by the basal melting distribution, but, although the ice shelf thins in the most of the simulations, there is little grounding line retreat. We find that the Lambert Glacier grounding line can retreat as much as 30 km if there is sufficient thinning of the ice shelf south of Clemence Massif, but none of the ocean models provide sufficiently high melt rates in that region. Overall, the increased accumulation computed by the atmosphere models outweighs ice stream acceleration so that the net contribution to sea level rise is negative.

1 Introduction

Climate change can affect an ice sheet by altering its mass balance directly through surface accumulation and melting, or indirectly through melting and refreezing on the ice shelf/ocean interface and the consequential dynamic thickening and thinning (van den Broeke et al., 2009; Williams et al., 2001; Huybrechts and de Wolde, 1999). So far the retreat and disintegration of ice shelves in the west and east coast of the Antarctica Peninsula as well as some of the most dramatic thinning and elevation changes observed in Pine Island Glacier are associated with atmospheric and oceanic warming (Scambos et al., 2000; Skvarca et al., 1999; Joughin et al., 2003; Shepherd et al., 2002). Mass change over the ice sheet will in turn affect the global sea level (van den Broeke et al., 2009): the rate of sea-level rise due to the present-day mass loss from Antarctica is about 0.25 mm yr^{-1} for 2000–2011 (Shepherd et al., 2012). These con-

cerns the application of numerical models that attempt to simulate the current state of ice sheets and their response to future climate forcing.

As one of the largest ice drainage systems in Antarctic (Rignot and Thomas, 2002) the Lambert Glacier–Amery Ice Shelf (LG-AIS) system plays a crucial role in determining the future responses of East Antarctica to climate change as it drains about 16 % of the grounded East Antarctica (Fricker et al., 2000). The grounded portion of the system is thought to be in balance or positive imbalance by numerous observations (Wen et al., 2006, 2008; Yu et al., 2010). The Amery Ice Shelf interacts with the ocean cavity beneath resulting in complex patterns of melting and refreezing (Galton-Fenzi et al., 2012). In total, 50 % of the mass (around $46.4 \pm 6.9\,\mathrm{Gt\,yr^{-1}}$) leaves the ice shelf through basal melting (Wen et al., 2010), with the remainder lost though calving events at the northern edge (Yu et al., 2010).

AIS has a relatively narrow shape comparing to the Ross Ice Shelf and the Ronne–Filchner Ice Shelf and its ice shelf front only accounts for 1.7 % of the total East Antarctic coastline (Budd et al., 1966). Several topographic features characterize the dynamics of AIS including:

(1) the Prince Charles Mountains in the west and Mawson Escarpment, Manning Nunataks and Reinbolt Hills in the east, which provide large lateral drag;

(2) the Clemence Massif (Hambrey and Dowdeswell, 1994), which is an elongated, mostly ice-free massif located at the south-eastern part of the ice shelf.

The AIS has long been considered a stable ice shelf that is currently undergoing a natural advance–calve–advance cycle (Fricker et al., 2002a, b). Observations of its mass balance (Wen et al., 2006, 2008; Yu et al., 2010) and model studies of the rift propagation process on its ice front (Larour et al., 2004; Bassis et al., 2005; MacAyeal et al., 2007) support that hypothesis. But the future state of the whole drainage system has large uncertainties under the influence of global warming and model studies can perhaps throw light on the future of the ice shelf and its adjacent glaciers.

In this study, we carried out dynamic simulations of the Lambert Glacier–Amery Ice Shelf (LG-AIS) system. Two factors govern the results of the projection when doing

dynamic simulations (Payne et al., 2013). One is the input climatic forcing; the other one is the issue of whether the ice sheet model can properly capture the character of the migration of the grounding line (GL) and the fast flow of the ice across the GL.

A set of previously published surface mass balance (SMB) and basal melt rate calculations were employed as climate forcing in this study. Two higher resolution atmospheric Models, LMDZ4 and RACMO2 (Agosta, 2012; Agosta et al., 2012; Ligtenberg et al., 2012), and two ocean models, BRIOS and FESOM (Beckmann et al., 1999; Timmermann et al., 2002; Timmermann and Helmer, 2013), are chosen to provide the SMB and basal melt rate respectively. They are driven by the boundary data computed by two Global Climate Models (GCMs), HadCM3 and ECHAM5 which are in turn driven by Green House Gases (GHG) Emission Scenarios E1 or A1B.

The ice sheet model used in this study employs adaptive mesh refinement (AMR) to obtain a non-uniform mesh that has finer spatial resolution where dynamics such as grounding line and fast flowing ice stream exist and coarser resolution where fine resolution is unnecessary. As the resolution of the mesh evolves with time to follow the GL (Cornford et al., 2012), this model is well suited to studying grounding line migration and dynamic thinning in the region of the Amery Ice Shelf.

Through the model simulation three specific subjects have been looked at in order to assess the responses of LG-AIS system to uncertain climate forcing in 21st and 22nd centuries. They are:

1. Investigating the dynamic changes of the LG-AIS system including ice thickness change, ice velocity change and grounding line migration under different climate forcing;
2. Estimating the responses of the changes of the LG-AIS system, namely its contribution to the global sea level.
3. Comparing the differing roles of SMB , basal melt rate and the topographic features on the dynamics of the LG-AIS system;

2 Methodology

2.1 Ice sheet model

The comprehensive description of the BISICLES adaptive mesh ice sheet model used in this study can be found in Cornford et al. (2012). BISICLES employs a vertically integrated model based on Schoof and Hindmarsh, 2010, which includes longitudinal and lateral strains and a simplified treatment of vertical shear strain, and is best suited to ice shelves and fast floating ice streams. It makes use of block-structured adaptive mesh refinement (AMR), supported by the Chombo C++ toolkit, to maintain fine resolution along the grounding line and in ice stream, and coarser resolution elsewhere (Colella et al., 2000). Meshes having grid cells with ∂x = 10, 5, or 2.5 km (a 3-level mesh) and a set of 4-level meshes with ∂x = 10, 5, 2.5, or 1.25 km have both applied in this study. A 2-level mesh covering the AIS region is shown in Fig. 1.

Ice thickness and bedrock topography data are drawn from the 5 km ALBMAP DEM (Le Brocq et al., 2010). The basic mask for the whole Antarctic is obtained from the Mosaic of Antarctic (MOA) coastline shape files (Haran et al., 2005; Scambos et al., 2007). Modifications have been made to the grounding line in order to smoothly combine the grounded ice sheet, which is largely from BEDMAP datasets (Lythe et al., 2001), with the ice shelf. The basal topography and marine bathymetry is based on the BEDMAP datasets but more data have been provided in ALBMAP data sets, especially bathymetry underneath ice shelves. The ice thickness data of grounded ice is produced through incorporation of the original BEDMAP ice thickness and the AGASEA/BBAS data (Vaughan et al., 2006; Holt et al., 2006). The ice shelf thickness is derived by hydrostatic assumption from surface elevations.

To initialize the model, we need to provide a basal friction coefficient field, along with temperature and enhancement factor fields to compute the effective viscosity. The ice temperature profile is provided by a three-dimensional thermo-mechanical higher-order model constructed by Pattyn (2010). The basal friction coefficient and enhancement factor are calculated by an optimization method similar to that of MacAyeal (1992),

Joughin et al. (2009) and Morlighem et al. (2010) which seeks to minimise the difference between the magnitude of modelled velocity and velocity data taken from InSAR observations acquired during the year 2007 to 2009 (Rignot et al., 2011a). Figure 2a shows the observed ice velocity of the LG-AIS system, while Fig. 2b shows the modelled velocity at the start of the simulation.

With the type of optimization we used we find high-frequency variation in the ice thinning (or thickening) rate, which are assumed to be artefacts of interpolation and other sources of error in the ice sheet geometry (Morlighem et al., 2011; Seroussi et al., 2011), or mismatch between the time at which the geometry and velocity were observed. So before carrying out all the targeted experiments we run (relax) the model for a period with a present day forcing to bring it closer to a steady-state. The relaxation is carried out in two stages. First we set the SMB to the 2000–2009 mean from the RACMO/HadCM3/E1 data, and the sub-shelf melt rate is chosen to keep the ice shelf in steady state. After 50 yr, we compute an accumulation rate M_s^0 required to keep the grounded ice in steady state, and a spatially smoothed melt rate M_b^0, decomposed into ambient and near grounding line components, which will keep the ice shelf close to steady state. We then run the model for 50 yr starting again from the initial state. The resulting ice sheet state is closer to, but not at, equilibrium, and we carry out all projections starting from this state, with SMB and melt rates computed by adding the perturbations described in the next section to M_s^0 and M_b^0.

2.2 Climate forcing

Table 1 shows the time-and-space averaged SMB and mean annual surface air temperature for each atmospheric forcing, and the melt rate and water temperature for the oceanic forcing. The surface temperature outputs obtained by all of the forcing combinations show increasing trends, especially that of the LMDZ4-HadCM3-A1B combination. Most of the SMB values increase slightly, with positive and growing SMB distributed over grounded ice. However, the water temperature beneath AIS exhibits a warming or cooling trend depending on the model. The BRIOS-HadCM3-E1 com-

bination has a temporal and spatial averaged warmest water temperature (−0.35°) beneath Amery Ice Shelf, and that given by the FESOM-ECHAM5-E1 combination is coldest (−1.78°). Most of the melt rate data exhibit a positive trend during the simulation period except for BRIOS-HadCM3-A1B and BRIOS-HadCM3-E1.

SMB and melt rates have been selected to drive 5 basic simulation cases (Table 1). Two Worst Case (WC) simulations have the smallest averaged SMB value (51.12 $\mathrm{Gt\,yr^{-1}}$) and the largest averaged basal melt rate (229.43 $\mathrm{Gt\,yr^{-1}}$ for WC-BRI and 221.77 $\mathrm{Gt\,yr^{-1}}$ for WC-FES). The Best Case (BC) simulation has the largest averaged SMB value (137.05 $\mathrm{Gt\,yr^{-1}}$) and the smallest averaged basal melt rate (23.77 $\mathrm{Gt\,yr^{-1}}$). Two neutral cases (N1 and N2) have also been chosen whose averaged SMB data and averaged melting data are close to the mean values among all the SMB and melt rate outputs. In addition, the cases with only SMB or melt rate anomalies (WC-SMB, WC-Melt, BC-SMB, BC-Melt, N1-SMB, N1-Melt, N2-SMB and N2-Melt) were carried out to investigate the influences separately. All the data of those 14 cases are applied to the ice sheet model as anomalies relative to their 1980–1989 temporal mean.

2.3 Experiment

In this study, we categorised the simulations into normal simulations and extreme simulations (Table 2). In normal simulations, 14 climate-driven simulations have been carried out by applying climate forcing as anomalies against the 1980–1990 average run to 2220 or 2100 (the forcing provided by combinations contain ECHAM5 are only up to 2100). In other words we assume that AIS was approximately in balance with the climate before the 1990s, as suggested by Rignot et al. (2011b), and construct both SMB and melt rate from the sum of the equilibrium rates M_{b}^{0} and M_{s}^{0} and the changes computed by the climate models. We need to run our simulations this way firstly because the ice sheet model state described in Sect. 2.1 is not near to equilibrium with respect to any of the climate models around 1980 and secondly because the climate models are not in close agreement for the 1980s. As the model ice sheet is not in perfect equilibrium even without climate perturbations, we also carry out a control run with constant forcing to quantify the model's drift (no anomalies are applied).

In the extreme simulations, intended to investigate the stability of the southern grounding line, we set the melt rate to 1000 $\mathrm{m\,yr^{-1}}$ in a portion of the ice shelf, effectively removing that part of the shelf entirely within a few years and run these simulations from 1980 to 2220. In the most extreme case, sensitive experiment S_0, the entire ice shelf is removed while in cases S_1–S_5 a region north of a line (shown in Fig. 2b) disappears.

All simulations we carried out on both 3-level and 4-level refined meshes, and selected simulations on 5-level refined meshes (with finest resolution ∂x = 625 m) to assess the effect of the resolution on the grounding line migration. The differences between simulations due to mesh resolution are no more than 12 % of mass imbalance.

3 Results and discussion

3.1 The response of LG-AIS system to different accumulation and melting inputs

The ice thickness changes of the LG-AIS system of all climate-driven simulations as well as the control run are shown in Fig. 3. Unsurprisingly, the pattern of thinning in the shelf is determined by the ocean model, with the SMB only cases resembling the control run, and the combined cases resembling those with no SMB anomaly. All the simulations show thinning in the northern part of the ice shelf and thickening in the southern part except for WC-FES (and WC-FES-Melt) and N1 (and N1-Melt). In the WC-BRI simulations (corresponding to the E1 climate scenario), high melt-rates are concentrated along the north-east and north-west of the shelf, leading to more than 400 m thinning there, while the region where the Fisher, Mellor and Lambert Glaciers converge into the ice shelf and downstream to Clemence Massif thickens most. The thickness of the entire ice shelf decreases in WC-FES and WC-FES-Melt most sig-

nificantly to the south of the Clemence Massif. In contrast, almost the entire ice shelf thickens in N1 (and N1-Melt) due to the re-freezing under the northern portion of the shelf produced by BRIOS with A1B scenario (Fig. 4).

The ice velocity along A-Aitof all climate-driven simulations in the final simulation year as well as the control and S_0 simulation are shown in Fig. 5. The ice shelf does not accelerate south of Clemence Massif except for the S_0 and WC-FES cases. The velocity of the WC-FES cases that is south of Clemence Massif increases to around half of that of the S_0 case. N1 cases accelerate downstream the most significantly as almost the entire ice shelf thickens in the end of the simulation.

From the results above, it can be concluded that the effects of the SMB inputs are minor comparing to that of basal melt rate in terms of thickness and velocity change. Besides, the distribution of melt rate seems as important as the total amount. It can be seen from Figs. 3 and 5 that both thickness and velocity changes of WC-FES are more dramatic than WC-BRI though they have similar amount of melt rate in total (Table 1). The melting of the former is distributed throughout the entire ice shelf and is larger between the southern grounding zone and Clemence Massif, in contrast, which of the later is distributed mainly at the northern part of the ice shelf and has slightly larger values along the northeast and northwest edge. The melting distribution, to some extent, has given a corresponding distribution of thickness change (Fig. 3). An odd changing pattern of velocity and ice thickness can also be found in N1 and N1-Melt that the ice shelf thickens and accelerates in the front at the end of the simulation as it can be seen that the ice shelf actually gains mass from beneath at the northern part (Fig. 4). And the basal accumulation only starts after about 2090 when the ice shelf also starts to thicken.

According to Yu et al. (2010), the melt rate of AIS decreases rapidly from the grounding zone to the ice shelf front and significant basal refreezing is detected in the downstream section. From preliminary studies (only three results are shown in Fig. 4), no melt rate distribution of all the model combinations have matched the observation exactly, which would cause large uncertainties to the projection of the LG-AIS system.

3.2 Grounding line migration

The distances of the GL migration of all simulations are displayed in Table 3. As the shape of GL is irregular we have only roughly considered the largest distance change of one point along the GL before and after the migration happen. The GL change of control run is shown in Fig. 6a. The GL changes of other normal simulations are similar. No significant migrations can be found in the results of all the normal simulations and the control run.

The southern GL of all the normal simulations except for WC-FES and WC-FES-Melt have advanced (less than 5 km) even though in certain cases the ice shelf has gone through dramatic thinning. The GL of the Charybdis Glacial basin (western GL) in some simulations retreats during the simulation period. The retreats of WC-BRI and WC-BRI-Melt are the most significant (> 5 km) among all the simulation cases.

In theory, the thinning of the ice shelf would cause buttressing loss which would cause immediately acceleration and thinning of the ice sheet (Dupont and Alley, 2005) and the GL retreat might be expected in response to buttressing lose (Rignot, 2002). However, even the two WC melt only cases do not give noticeable GL retreat. It raises the assumption that the GL migration of Amery Ice Shelf is more complicated due to certain topographic features and its narrow shape. In order to investigate the buttressing providing we did sensitivity tests by removing the ice shelf stepwise to different extents.

The results of the retreat distance of the southern and western GL are shown in Table 3. By removing the entire ice shelf, the grounding line has retreated for just 30.5 km inland which is relatively small comparing to the removal of the entire ice shelf in Pine Island area (retreats for 150 km) (Payne et al., 2013). When we remove the ice shelf to some point approximately in the middle (S_1) of the ice shelf the final southern GL remains at the same position as the initial year, namely the GL neither retreat nor advance. By removing the ice shelf gradually further inland the GL start to retreat. Through comparison between the GL migration of S_3, which melts the ice shelf right at

the Clemence Massif, and S_4 the significance of Clemence Massif for the buttressing of the grounded ice can be found. Only when the ice shelf is removed right behind the Clemence Massif (S_4) does the southern GL retreat dramatically (> 10 km) much as in the S_0 simulation (Fig. 5).

Therefore, we suggest that the buttressing for the grounded ice in the southern basin is largely provided by Clemence Massif. And the buttressing provided by a single massif may be also magnified as AIS is confined between high mountains with a narrow distance between the two sides. The role the Clemence Massif played in buttressing providing needs further investigation.

The retreat of the western GL is rather limited by the topography that even removing the entire section in front of it does not cause retreat larger than 10 km.

3.3 The contribution of Amery Ice Shelf to the global sea level

The evolution of the volume of ice above flotation (VAF) integrated over the entire LG-AIS system, which is directly related to global sea level change, is shown in Fig. 7. Note that the control run is not in steady state because of the smoothing of the mass flux data, as described in Sect. 2.1, so that model drift amounts to 1.1×10^3 km^3 (−2.7 mm SLR). VAF increases in all but the WC-FES and WC-FES-Melt simulations. In these worst-case simulations, VAF reaches a peak – around 2125, then drops, by 0.4×10^3 km^3 (1.0 mm SLR) by the end of the simulation. The majority of the remaining simulations show a positive change in VAF: as much as 2.2×10^3 km^3 (−5.7 mm SLR) in the best case (BC, BC-SMB) simulations.

Almost all the simulations show a decrease of the global sea level at the end of the simulation (Table 3).The results of the control run may lower the global sea level by 2.79 mm. And the steepest falling is given by BC and BC-SMB that will decrease the global sea level by 5.58 mm at the end of 2100. The only simulations that cause global sea level rising are the WC-FES (increase by 1.01 mm) and WC-FES-Melt (increase by 1.01 mm) case.

4 Conclusions

We have presented the modelling results of Lambert Glacier–Amery Ice Shelf system driven by different combinations of SMB and melt rate inputs provided by several climate models. The ice thickness and velocity of Amery Ice Shelf is influenced mainly by basal melt rates rather than SMB as the majority of the positive SMB located on the grounded ice. The grounding line migration is more sensitive to the distribution of the basal melting. Grounding line retreat noticeably only if melt rates south of Clemence Massif are greater than 1000 m yr^{-1} Positive SMB, increasing Tamean (Table 1) and VAF change (Fig. 7) may suggest that the LG-AIS system is unlikely to become a big contributor to the global sea level rise in the future even under warm climate. However the relationship between surface warming and the quantity and distribution of SMB in LG-AIS system needs further investigation.

Acknowledgements. The authors would like to thank Daniel F. Martin for his contributions to the BISICLES code. BISICLES is jointly developed at Lawrence Berkeley National Laboratory, California, USA and the University of Bristol, UK with financial support provided through Scientific Discovery through Advanced Computing (SciDAC) program funded by US Department of Energy, Office of Science, Advanced Scientific Computing Research and Biological and Environmental Research and the UK Natural Environment Research Council. Thanks to CSC-IT Centre for Science Ltd, Espoo, Finland providing the super cluster for carrying on the model simulations.

References

Agosta, C.: Evolution du bilan de masse de surface antarctique par regionalization physique et conséquences sur les variations du niveau des mers, Université de Grenoble, 2012.

Agosta, C., Favier, V., Krinner, G., Gallée, H, Fettweis, X., and Genthon, C.: High-resolution modelling of the Antarctic surface mass balance, application for the 20th, 21st and 22nd centuries. Paper presented at European Geosciences Union General Assembly 2013, Vienne, Autriche, 2013.

Bassis, N. J., Coleman, R., Fricker, H. A., and Minster, J. B.: Episodic propagation of a rift on the Amery Ice Shelf, East Antarctica, Geophys. Res. Lett., 32, L06502, doi:10.1029/2004GL022048, 2005.

Beckmann, A., Hellmer, H. H., and Timmermann, R.: A numerical model of the Weddell Sea: large-scale circulation and water mass distribution, J. Geophys. Res.-Oceans, 104, 23375–23391, 1999.

Budd, W. F., Landon-Smith, I. H., and Wishart, E.: The Amery Ice Shelf, in: Physics of Snow and Ice: Proceedings of the International Conference on Low Temperature Science, edited by: Oura, H., Institute of Low Temperature Science, Sapporo, 447–467, 1966.

Colella, P., Graves, D. T., Keen, N., Ligocki, T. J., Martin, D. F., McCorquodale, P., Modiano, D., Schwartz, P., Sternberg, T., and Straalen, B. V.: Chombo Software Package for AMR Applications – Design Document, unpublished, 2000.

Cornford, S. L., Martin, D. F., Graves, D. T., Ranken, D. F., Le Brocq, A. M., Gladstone, R. M., Payne, A. J., Ng, E. G., and Lipscomb, W. H.: Adaptive mesh, finite volume modeling of marine ice sheets, J. Comput. Phys., 232, 529–549, 2012.

Dupont, T. K. and Alley, R.: Assessment of the importance of ice shelf buttressing to ice-sheet flow, Geophys. Res. Lett., 32, L04503, doi:10.1029/2004GL022024 , 2005.

Fricker, H. A., Hyland, G., Coleman, R., and Young, N. W.: Digital elevation models for the Lambert Glacier–Amery Ice Shelf system, East Antarctica, from ERS-1 satellite radar altimetry, J. Glaciol., 46, 553–560, 2000.

Fricker, H. A., Allison, I., Craven, M., Hyland, G., Ruddell, A., Young, N., Coleman, R., King, M., Krebs, K., and Popov, S.: Redefinition of the Amery Ice Shelf, East Antarctica, grounding zone, J. Geophys. Res., 107, 2092, ECV 1-1-ECV 1-9, doi:10.1029/2001JB000383, 2002a.

Fricker, H. A., Young, N. W., Allison, I., and Coleman, R.: Iceberg calving from the Amery Ice Shelf, East Antarctica, Ann. Glaciol., 34, 241–246, doi:10.3189/172756402781817581, 2002b.

Fortuin, J. P. F. and Oerlemans, J..: Parameterization of the annual surface temperature and mass balance of Antarctica, Ann. Glaciol., 14, 78–84, 1990.

Galton-Fenzi, B. K., Hunter, J. R., Coleman, R., Marsland, S., and Warner, R. C.: Modeling the Basal Melting and Marine Ice Accretion of the Amery Ice Shelf, J. Geophys. Res., doi:10.1029/2012JC008214, in press, 2012.

Hambrey, M. J. and Dowdeswell, J. A.: Flow regime of the Lambert Glacier–Amery Ice Shelf system, Antarctica: structural evidence from Landsat imagery, Ann. Glaciol., 20, 401–406, 1994.

Haran, T., Bohlander, J., Scambos, T., Painter, T., and Fahnestock, M. (compilers): MODIS mosaic of Antarctica (MOA) image map, National Snow and Ice Data Center, Digital media, Boulder, Colorado, USA, 2005 (updated 2006).

Holt, J. W., Blankenship, D. D., Morse, D. L., Young, D. A., Peters, M. E., Kempf, S. D., Richter, T. G., Vaughan, D. G., and Corr, H. F. J.: New boundary conditions for the West Antarctic Ice Sheet: subglacial topography of the Thwaites and Smith glacier catchments, Geophys. Res. Lett., 33, L09502, doi:10.1029/2005GL025561, 2006.

Howat, I. M., Ahn, Y., Joughin, I., van de Broeke, M. R., Lenaerts, J. T. M. and Smith, B.: Mass balance of Greenland's three largest outlet glaciers, 2000–2010, Geophys. Res. lett., 38, L12501, doi:10.1029/2011GL047565, 2011.

Huybrechts, P. and de Wolde, J.: The dynamic response of the Greenland and Antarctic Ice Sheets to multiple-century climatic warming, J. Climate., 12, 2169–2188, 1999.

Joughin, I., Rignot, E., Rosanova, C. E., Lucchitta, B. K., and Bohlander, J.: Timing of recent accelerations of Pine Island Glacier, Antarctica, Geophys. Res. Lett., 30, doi:10.1029/2003GL017609, 2003.

Joughin, I., Tulaczyk, S., Bamber, J. L., Blankenship, D., Holt, J. W., Scambos, T., and Vaughan, D. G.: Basal conditions for Pine Island and Thwaites Glaciers, West Antarctica, determined using satellite and airborne data, J. Glaciol. 55, 245–257, 2009.

Larour, E., Rignot, E., and Aubry, D.: Modelling of rift propagation on Ronne Ice Shelf, Antarctica, and sensitivity to climate change, Geophys. Res. Lett., 31, L16404, doi:10.1029/2004GL020077, 2004.

Le Brocq, A. M., Payne, A. J., and Vieli, A.: An improved Antarctic dataset for high resolution numerical ice sheet models (ALBMAP v1), Earth Syst. Sci. Data, 2, 247–260, doi:10.5194/essd-2-247-2010, 2010.

Ligtenberg, S. R. M., van de Berg, W. J., van den Broeke, M. R., Rae, J. G. L., and van Meijgaard, E.: Future surface mass balance of the Antarctic ice sheet and its influence on sea level change, simulated by a regional atmospheric climate model, Clim. Dynam., 41, 867–884, doi:10.1007/s00382-013-1749-1, 2013.

Lythe, M. B., Vaughan, D. G., and the BEDMAP Consortium: BEDMAP: a new ice thickness and subglacial topographic model of Antarctica, J. Geophys. Res.-Sol. Ea., 106, 11335–11351, 2001.

McMahon, K. L.: Seismic surveys of the Amery Ice Shelf, East Antarctica: an investigation of meteoric and marine ice, the ocean cavity and the anisotropic crystalline structure of strained ice, Ph.D. Thesis, Dept. of Earth and Planetary Sciences, Macquarie University, Australia, 231 pp., 2012.

MacAyeal, D. R.: The basal stress distribution of ice stream E, Antarctica, inferred by control methods, J. Geophys. Res., 97, 595–603. 1992

MacAyeal, D. R., Okal, E. A., Aster, R. C., Bassis, J. N., Brunt, K. M., Cathles, L. M., Drucker, R., Fricker, H. A., Kim, Y., Martin, S., Okal, M. H., Sergienko, O. V., Sponsler, M. P., and Thom, J. E.: Transoceanic wave propagation links iceberg calving margins of Antarctica with storms in tropics and Northern Hemisphere, Geophys. Res. Lett., 33, L17502, doi:10.1029/2006GL027235, 2007.

Morlighem, M., Rignot, E., Seroussi, H., Larour, E., Ben Dhia, H., and Aubry, D.: Spatial patterns of basal drag inferred using control methods from a full-Stokes and simpler models for Pine Island Glacier, West Antarctica, Geophys. Res. Lett., 37, L14502, doi:10.1029/2010GL043853, 2010.

Morlighem, M., Rignot, E., Seroussi, H., Larour, E., Ben Dhia, H., and Aubry, D.: A mass conservation approach for mapping glacier ice thickness, Geophys. Res. Lett., 38, L19503, doi:10.1029/2011GL048659, 2011.

Pattyn, F.: Antarctic subglacial conditions inferred from a hybrid ice sheet/ice stream model, Earth Planet. Sc. Lett., 295, 451–461, doi:10.1016/j.epsl.2010.04.025, 2010.

Payne, A. J., Cornford, S. L., Martin, D. F., Agosta, C., van den Broeke, M. R., Edwards, T. L., Gladstone, R. M., Hellmer, H. H., Krinner, G., Le Brocq, A. M., Ligtenberg, S. R. M., Lipscomb, W. H., Ng, E. G., Shannon, S. R., Timmerman, R., and Vaughan, D. G.: Impact of uncertain climate forcing on projections of the West Antarctic ice sheet over the 21st and 22nd centuries, Earth. Planet. Sc. Lett., submitted, 2013.

Rignot, E.: Ice-shelf changes in Pine Island Bay, Antarctica, 1947–2000, J. Glaciol., 48, 247–256, 2002.

Rignot, E. and Jacobs, S.: Rapid bottom melting widespread near Antarctic Ice Sheet grounding lines, Science, 296, 2020–2023, 2002.

Rignot, E. and Thomas, R. H.: Mass balance of Polar Ice Sheets, Science, 297, 1502–1506, 2002.

Rignot, E., Mouginot, J., and Scheuchl, B.: Ice flow of the Antarctic Ice Sheet, Science, 521, 1427–1430, 2011a.

Rignot, E., Velicogna, I., van den Broeke, M. R., Monaghan, A., and Lenaerts, J.: Acceleration of the contribution of the Greenland and Antarctic ice sheets to sea level rise, Earth Planet. Sc. Lett., L05503, doi:10.1029/2011GL046583, 2011b.

Robin, G. de Q: Ice cores and climatic change, Philos. T. Roy. Soc. B., 280, 143–168, 1977.

Scambos, T. A., Hulbe, C., Fahnestock, M., and Bohlander, J.: The link between climate warming and break-up of ice shelves in the Antarctic Peninsula, J. Glaciol., 46, 516–530, 2000.

Scambos, T. A., Haran, T. M., Fahnestock, M. A., Painter, T. H., and Bohlander, J.: MODIS-based Mosaic of Antarctica (MOA) data sets: continent-wide surface morphology and snow grain size, Remote Sens. Environ., 111, 242–257, 2007.

Schoof, C. and Hindmarsh, R. C. A.: Thin-film flows with wall slip: an asymptotic analysis of higher order glacier flow models, Q. J. Mech. Appl. Math., 63, 73–114, doi:10.1093/qjmam/hbp025, 2010.

Seroussi, H., Morlighem, M., Rignot, E., Larour, E., Ben Dhia, H., Aubry, D., and Kristensen, S. S.: Ice flux divergence anomalies on 79north Glacier, Greenland, Geophys. Res. Lett., 38, L09501, doi:10.1029/2011GL047338, 2011.

Shepherd, A., Wingham, D. J., and Mansley, J. A. D.: Inland thinning of the Amundsen Sea sector, West Antarctica, Geophys. Res. Lett., 29, 1364, doi:10.1029/2001GL014183, 2002.

Shepherd, A., Ivins, E., Geruo, A., Barletta, V., Bentley, M., Bettadpur, S., Briggs, K., Bromwich, D., Forsberg, R., Galin, N., Horwath, M., Jacobs, S., Joughin, I., King, M., Lenaerts, J., Li, J., Ligtenberg, S., Luckman, A., Luthcke, S., McMillan, M., Meister, R., Milne, G., Mouginot, J., Muir, A., Nicolas, J., Paden, J., Payne, A., Pritchard, H., Rignot, E., Rott, H., Sorensen, L., Scambos, T., Scheuchl, B., Schrama, E., Smith, B., Sundal, A., van Angelen, J., van de Berg, W., van den Broeke, M., Vaughan, D., Velicogna, I., Wahr, J., Whitehouse, P., Wingham, D., Yi, D., Young, D., and Zwally, H.: A reconciled estimate of ice-sheet mass balance, Science, 338, 1183–1189, doi:10.1126/science.1228102, 2012.

Skvarca, P., Rack, W., and Rott, H.: 34 yr satellite time series to monitor characteristics, extent and dynamics of Larsen B, Antarctic Peninsula, Ann. Glaciol. 29, 255–260, 1999.

Timmermann, R. and Helmer, H. H.: Southern Ocean warming and increased ice shelf basal melting in the 21st and 22nd centuries based on coupled ice-ocean finite element modelling, Ocean Dyn., accepted, 2013.

Timmermann, R., Hellmer, H. H., and Beckmann, A.: Simulations of ice-ocean dynamics in the Weddell Sea. 2. Interannual variability 1985–1993. J. Geophys. Res. 107, 11-1-11-9, doi:10.1029/2000JC000742, 2002.

van den Broeke, M. R., Bamber, J., Ettema, J., Rignot, E., Schrama, E., van de Berg, W. J., van Meijgaard, E., Velicogna, I., and Wouters, B.: Partitioning recent Greenland mass loss, Science., 326, 984–986, 2009.

Vaughan, D. G., Corr, H. F. J., Ferraccioli, F., Frearson, N., O'Hare, A., Mach, D., Holt, J., Blankenship, D., Morse, D., and Young, D. A.: New boundary conditions for the West Antarctic ice sheet: subglacial topography beneath Pine Island Glacier, Geophys. Res. Lett., 33, L09501, doi:10.1029/2005GL025588, 2006.

Velicogna, I.: Increasing rates of ice mass loss from the Greenland and Antarctic ice sheets revealed by GRACE, Geophys. Res. Lett., 36, L19503, doi:10.1029/2009GL040222, 2009.

Wen, J., Jezek, K. C., Monaghan, A. J., Sun, B., Ren, J., and Huybrechts, P.: Accumulation variability and mass budgets of the Lambert Glacier–Amery Ice Shelf system at high elevations, Ann. Glaciol., 43, 351–360, 2006.

Wen, J., Wang, Y., Liu, J., Jezek, K. C., Huybrechts, P., Csatho, B. M., Farness, P., and Sun, B.: Mass budget of the grounded ice in Lambert Glacier–Amery Ice Shelf system, Ann. Glaciol., 48, 193–197, 2008.

Wen, J., Wang, Y., Wang, W., Jezek, K. C., Liu, H., and Allison, I.: Basal melting and freezing under the Amery Ice Shelf, East Antarctica, J. Glaciol., 56, 81–90, 2010.

Williams, M. J. M., Grosfeld, K., Warner, R. C., Gerdes, R., and Determann, J.: Ocean circulation and ice-ocean interaction beneath the Amery Ice Shelf, Antarctic, J. Geophys. Res., 106, 383–339, 2001.

Yu, J., Liu, H., Jezek, K. C., Warner, R. C., and Wen, J.: Analysis of velocity field, mass balance, and basal melt of the Lambert Glacier–Amery Ice Shelf system by incorporating Radarsat SAR interferometry and ICESat laser altimetry measurements, J. Geophys. Res., 115, B11102, doi:10.1029/2010JB007456, 2010.

Table 1. Means and linear squares regression trends of different period from different RCMs outputs time series.

Model	Period	Parameter	Temporal Mean(LA) ($Gtyr^{-1}$)	Temporal Mean(GI) ($Gtyr^{-1}$)	Temporal Mean(FI) ($Gtyr^{-1}$)	Trend (LA)	Trend (GI)	Trend (FI)
LMDZ4-HadCM3-A1B (BC)	**2000–2199**	**SMB**	**137.05**	**123.19**	**13.84**	**0.2746**	**0.2673**	**0.0074**
	2000–2199	Tamean	−32.59			0.0217		
LMDZ4-HadCM3-E1	2000–2199	SMB	121.10	105.30	15.78	−0.0023	0.0020	−0.0042
	2000–2199	Tamean	−34.13			0.0023		
LMDZ4-ECHAM5-E1 (N2)	**2000–2099**	**SMB**	**111.82**	**95.66**	**16.14**	**0.0549**	**0.0558**	**−0.0010**
	2000–2099	Tamean	−34.71			0.0079		
RACMO-HadCM3-A1B (N1)	**2000–2199**	**SMB**	**57.98**	**53.57**	**4.40**	**0.0937**	**0.0876**	**0.0061**
RACMO-HadCM3-E1 (WC)	**2000–2199**	**SMB**	**51.12**	**47.20**	**3.91**	**0.0279**	**0.0244**	**0.0035**
RACMO-ECHAM5-A1B	2000–2099	SMB	56.72	51.45	5.25	0.0770	0.0744	0.0026
RACMO-ECHAM5-E1	2000–2099	SMB	52.97	48.19	4.77	0.0588	0.0528	0.0588
BRIOS-HadCM3-A1B (N1)	**2000–2199**	**Melt Rate**			**130.54**			**−1.3991**
	2000–2199	Water Temperature	−0.741			−0.0055		
BRIOS-HadCM3-E1(WC-BRI)	**2000–2199**	**Melt Rate**			**229.43**			**−0.1320**
	2000–2199	Water Temperature	−0.3478			−0.004		
BRIOS-ECHAM5-A1B	2000–2099	Melt Rate			71.93			0.8309
	2000–2099	Water Temperature	−0.9369			0.0066	0.0199	0.0199
BRIOS-ECHAM5-E1 (N2)	**2000–2199**	**Melt Rate**			**64.00**			**0.3655**
	2000–2199	Water Temperature	−0.9837			0.0033	0.0072	0.0072
FESOM-HadCM3-A1B(WC-FES)	**2000–2199**	**Melt Rate**			**221.77**			**2.4314**
	2000–2199	Water Temperature	−0.7686			0.0072		
FESOM-ECHAM5-A1B	2000–2099	Melt Rate			25.07			0.0766
	2000–2099	Water Temperature	−1.7759			0.0004	0.0004	0.0004
FESOM-ECHAM5-E1 (BC)	**2000–2199**	**Melt Rate**			**23.78**			**0.0248**
	2000–2199	Water Temperature	−1.7837			−0.0001	−0.0041	−0.0041

Table 2. Simulation combinations selected from the outputs of the RCMs and simulation period used in model study. The melt rate of Sensitive test 1–5 are set to be 1000 m yr^{-1} beneath the part that needs to be removes and remain the steady state melt rate beneath the rest part of the ice shelf.

			SMB Data	Basal Melting Data	Simulation Period
Normal Simulation	Control Simulation	Control	Amery-balance-SMB	Amery-balance-melt	1980–2220
	Climate-Driven Simulation	Worst Case-BRIOS (WC-BRI)	RACMO-HadCM3-E1	BRIOS-HadCM3-E1	1980–2220
		Worst Case-FESOM (WC-FES)	RACMO-HadCM3-E1	FESOM-HadCM3-A1B	1980–2220
		Best Case (BC)	LMDZ4-HadCM3-A1B	FESOM-ECHAM5-E1	1980–2100
		Neutral Case 1 (N1)	RACMO-HadCM3-A1B	BRIOS-HadCM3-A1B	1980–2220
		Neutral Case 2 (N2)	LMDZ4-ECHAM5-E1	BRIOS-ECHAM5-E1	1980–2100
		Worst Case SMB only (WC-SMB)	RACMO-HadCM3-E1		1980–2220
		Best Case SMB only (BC-SMB)	LMDZ4-HadCM3-A1B		1980–2220
		Neutral Case 1 SMB only (N1-SMB)	RACMO-HadCM3-A1B		1980–2220
		Neutral Case 2 SMB only (N2-SMB)	LMDZ4-ECHAM5-E1		1980–2100
		Worst Case-BRIOS Melt only (WC-BRI-melt)		BRIOS-HadCM3-E1	1980–2220
		Worst Case-FESOM Melt only (WC-FES-melt)		FESOM-HadCM3-A1B	1980–2220
		Best Case Melt only (BC-melt)		FESOM-ECHAM5-E1	1980–2100
		Neutral Case 1 Melt only (N1-melt)		BRIOS-HadCM3-A1B	1980–2220
		Neutral Case 2 Melt only (N2-melt)		BRIOS-ECHAM5-E1	1980–2100
Extreme		Remove-ice shelf	Amery-balance-SMB	1000	1980–2220
		Sensitive Test 1 (S_1)	Amery-balance-SMB	1000 + Amery-balance-melt	1980–2220
		Sensitive Test 2 (S_2)	Amery-balance-SMB	1000 + Amery-balance-melt	1980–2220
		Sensitive Test 3 (S_3)	Amery-balance-SMB	1000 + Amery-balance-melt	1980–2220
		Sensitive Test 4 (S_4)	Amery-balance-SMB	1000 + Amery-balance-melt	1980–2220
		Sensitive Test 5 (S_5)	Amery-balance-SMB	1000 + Amery-balance-melt	1980–2220

Table 3. Summaries of GL change and VAF change of each simulation case.

Experiment	G.L. advance southern (km)	G.L. advance western (km)	Initial VAF ($\times 10^6$ km^3)	Final VAF ($\times 10^6$ km^3)	VAF Gain ($\times 10^3$ km^3)	Sea level Change (mm)
Control	5	0	2.8902	2.8913	1.10	−2.79
WC-BRI	5	−5.3	2.8902	2.8908	0.60	−1.52
WC-FES	−6.3	−2.5	2.8902	2.8898	−0.40	1.01
WC-BRI-melt	2.5	−6.3	2.8902	2.8908	0.60	−1.52
WC-FES-melt	−3.8	−2.5	2.8903	2.8900	−0.30	1.01
WC-SMB	5	0	2.8902	2.8913	1.10	−2.79
BC	2.5	0	2.8902	2.8924	2.20	−5.58
BC-melt	2.5	0	2.8902	2.8910	0.80	−2.03
BC-SMB	5	0	2.8902	2.8923	2.10	−5.32
N1	2.5	−2.5	2.8902	2.8928	2.60	−6.59
N1-melt	5	−2.5	2.8902	2.8912	1.00	−2.53
N1-SMB	5	0	2.8902	2.8929	2.70	−6.84
N2	2.5	−2.5	2.8902	2.8912	1.00	−2.54
N2-melt	2.5	−2.5	2.8902	2.8909	0.70	−1.78
N2-SMB	5	0	2.8902	2.8911	0.90	−2.28
Sensitive test 1	0	−7.6	2.8901	\	\	\
Sensitive test 2	−2.5	−7.6	2.8901	\	\	\
Sensitive test 3	−2.5	−7.6	2.8901	\	\	\
Sensitive test 4	−16.3	−7.6	2.8901	\	\	\
Sensitive test 5	−21.3	−7.6	2.8901	\	\	\
Sensitive test 0	−32.5	−9.5	2.8901	2.8868	−3.30	8.36

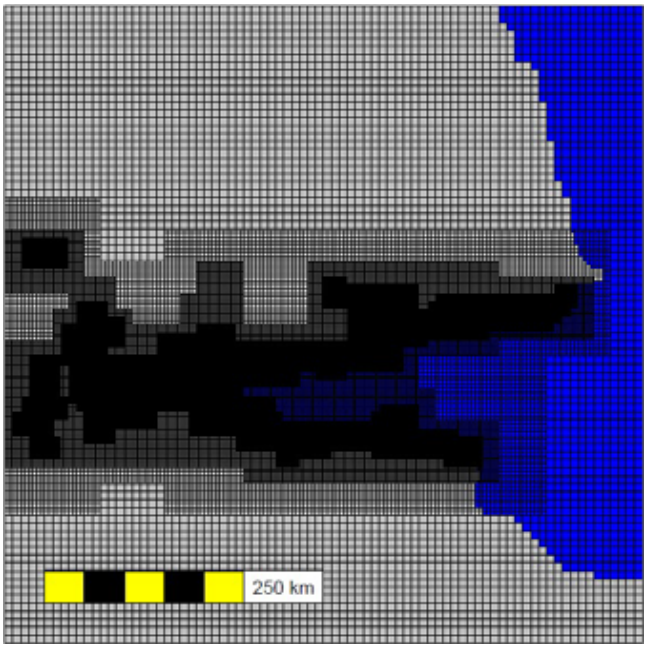

Fig. 1. The mesh in AIS region of a 2 level refinement. The finest solution (625 km) follows the grounding line.

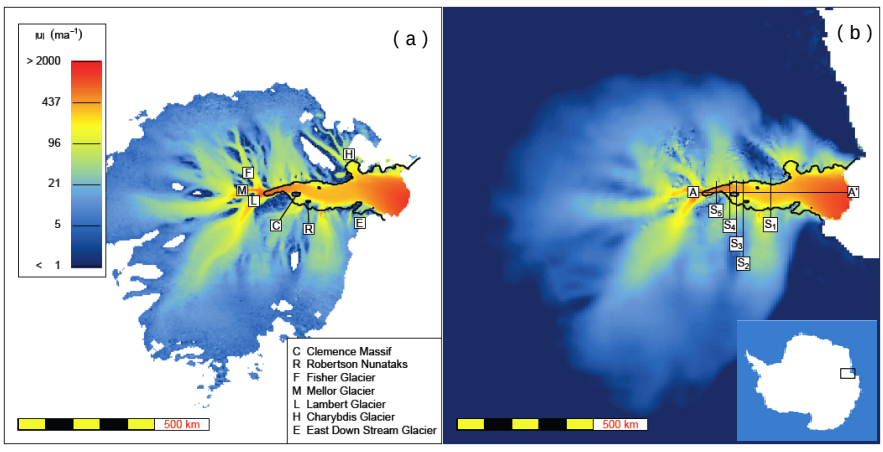

Fig. 2. Comparison between observational velocity and modeled velocity. **(a)** Observational velocity map obtained by multiple satellites InSAR acquired during the year 2007 to 2009 (Rignot et al., 2011). **(b)** Modeled velocity constrained using control method to match the observational velocity map. The longitudinal profile (A–A′) along which the ice thickness and ice velocity are compared are presented on the map.

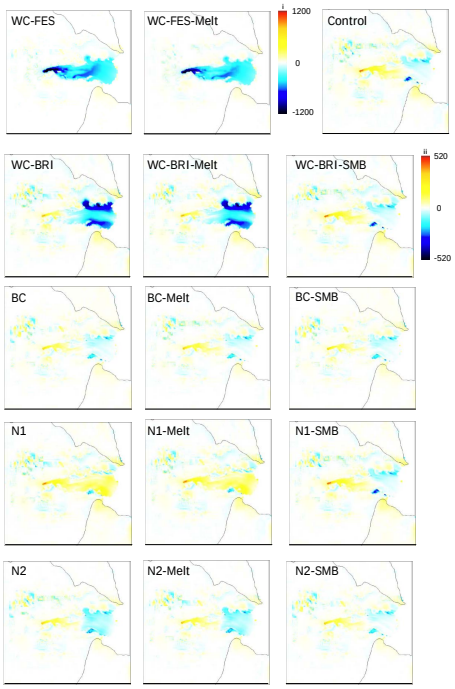

Fig. 3. The ice thickness changes of the Amery Ice Shelf at the end of the simulations. For N2, N2-Melt, N2-SMB and BC, BC-Melt, BC-SMB, the final simulation year are 2100. And for the other simulation cases, the final simulation year is 2200. WC-FES and WC-BRI have the same SMB input. The plots WC-FES and WC-FES-Melt refer to legend i and the rest of the plots refer to legend ii.

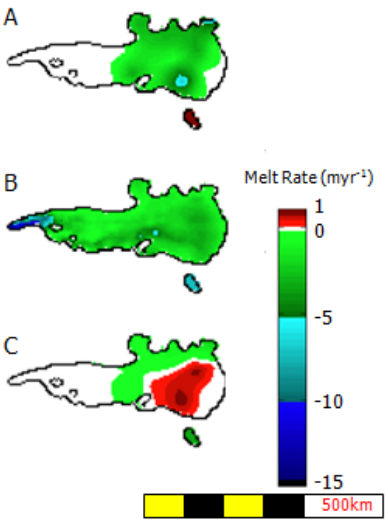

Fig. 4. The temporal mean basal melt rate from 1980 to 2200 of **(A)** WC-BRI; **(B)** WC-FES; **(C)** N1.

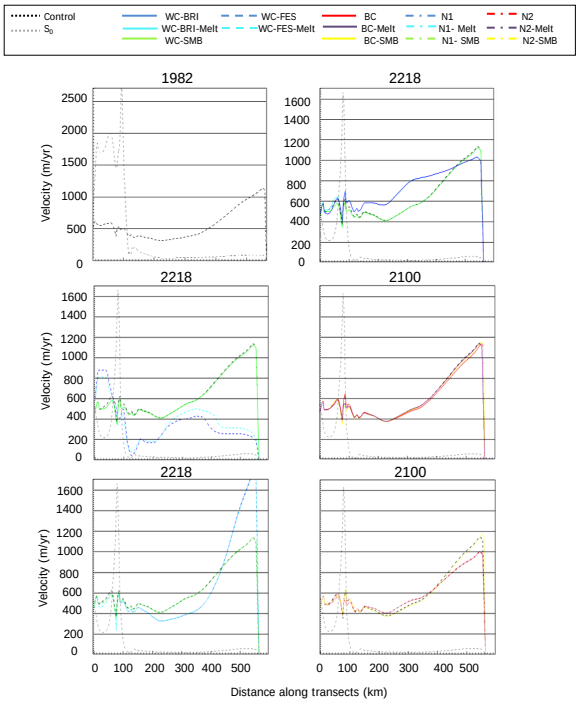

Fig. 5. Ice velocity of different simulation cases in different time period along longitudinal profile A–A′ (left 2 columns). The year of the simulations are marked above the plots. All the normal simulations have the same initial position (in the year 1982) with control run. For N2, N2-Melt, N2-SMB and BC, BC-Melt, BC-SMB, the final simulation year are 2100. And for the other simulation cases, the final simulation year is 2200.

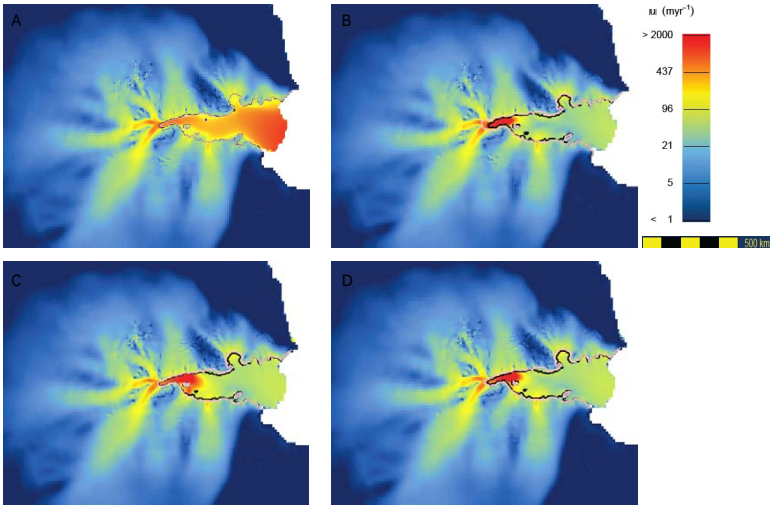

Fig. 6. Grounding line migration of the AIS in **(A)** control run, **(B)** S_0 simulation, **(C)** S_3 simulation, **(D)** S_4 simulation.

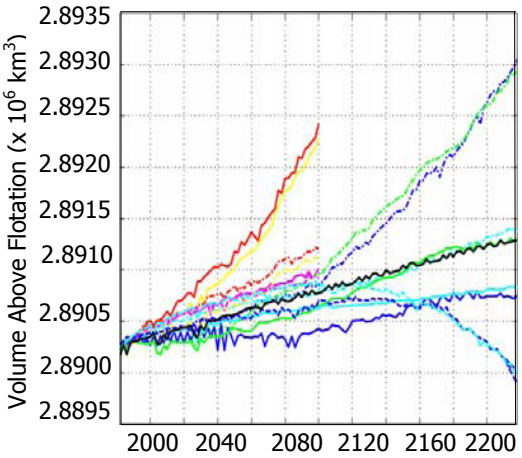

Fig. 7. The ice mass changes of the LG-AIS system over simulation period expressed as VAF. Different curves show the results of different simulation cases. The legend can be found in Fig. 4.